Biophysical Journal Volume 96 May 2009 4249–4259

Micro-PTV Measurement of the Fluid Shear Stress Acting on Adherent Leukocytes In Vivo

John E. Pickard[†] and Klaus Ley[†‡*]

[†]Department of Biomedical Engineering, University of Virginia, Charlottesville, Virginia; and [‡]La Jolla Institute for Allergy and Immunology, La Jolla, California

ABSTRACT Leukocyte adhesion is determined by the balance between molecular adhesive forces and convective dispersive forces. A key parameter influencing leukocyte adhesion is the shear stress acting on the leukocyte. This measure is indispensable for determining the molecular bond forces and estimating cell deformation. To experimentally determine this shear stress, we used microparticle tracking velocimetry analyzing more than 24,000 images of 0.5 μm fluorescent microbeads flowing within mildly inflamed postcapillary venules of the cremaster muscle in vivo. Green fluorescent protein, expressed under the lysozyme-M promoter, made leukocytes visible. After applying stringent quality criteria, 3 of 69 recordings were fully analyzed. We show that endothelial cells, but not leukocytes, are covered by a significant surface layer. The wall shear rate is nearly zero near the adherent arc of each leukocyte and reaches a maximum at the apex. This peak shear rate is 2–6-fold higher than the wall shear rate in the absence of a leukocyte. Microbead trajectories show a systematic deviation toward and away from the microvessel axis upstream and downstream from the leukocyte, respectively. The flow field around adherent leukocytes in vivo allows more accurate estimates of bond forces in rolling and adherent leukocytes and improved modeling studies.

INTRODUCTION

In acute and chronic inflammation, leukocyte-endothelium adhesion occurs despite disrupting shear forces which work to dislodge the white blood cell from the vessel wall. Binding events between molecules expressed on inflamed endothelial cells and their ligands on blood leukocytes generate adhesive forces, which resist the convective hemodynamic forces imparted by flowing blood. When these forces are almost in balance, leukocytes show rolling behavior, a motion characterized by molecular bond formation at the leading edge and peeling at the trailing edge (1). This force balance is a key determinant of the cell's rolling velocity (2,3) and its propensity to become adherent and is therefore a crucial component to the overall effectiveness of the inflammatory response. The dynamic adhesion process has been extensively studied with computational modeling of molecular bonds that cooperate to resist the fluid shear forces (4,5). There has been much speculation into the types, numbers, and spacing of bonds required to support adhesion and rolling and these simulations can help to answer these fundamental questions. Similarly, the complex fluid dynamics system of a deformable cell within a viscous non-Newtonian fluid has been a challenging problem of great interest (7–9,27). These computational findings depend critically on the assumption of the imparted fluid shear force, a parameter with limited experimental measurements.

The most common shear force estimation is based on an analytical solution for a rigid sphere adhered to a planar wall in Newtonian shear flow (10). However, leukocytes are deformable cells that interact within cylindrical microvessels under non-Newtonian blood flow. Leukocytes rarely adhere as spheres due to luminal drag forces deforming the cell to a tear drop shape (11) which, according to a simple one-dimensional geometric model, reduces fluid drag (12). In vivo, the average force per adherent leukocyte has been calculated from differential pressure measurements and a shear stress estimate based on Newtonian mechanics (12). Computational fluid dynamics (CFD) studies have provided exact force calculations for spherical, hemispherical, and tear drop shaped objects within parallel-plate flow chamber systems (13,14) and for deformed spheres within cylindrical tubes (7,15). One limitation of these approaches is that they must assume Newtonian fluids with uniform viscosity, which is not a good approximation of blood (16). Other models have explored the dynamic nature of cell-deformation under shear flow studying the time-dependence of the fluid-forces and yielding tear drop shaped cells within parallel-plate chamber flow (8,9,17).

Unfortunately, not many studies have successfully incorporated the non-Newtonian nature of blood. In vessels smaller than 100 μm, the particulate nature of the red blood cells (RBC) suspended in plasma causes non-Newtonian effects in the cross-sectional fluid velocity profile (18). Wall effects induce a nonuniform hematocrit, or volume fraction of RBC, manifested as a lateral migration of erythrocytes (19–21). This effect combines with cell aggregation and deformability to produce a blunted cross-sectional velocity profile in arterioles (22) and venules (16,23). The region near the endothelial surface and around rolling or adherent leukocytes is completely depleted of erythrocytes, forming a cell-free or plasma layer (24,25). Chapman and Cokelet devised a large scale model by matching Reynolds numbers and modeling RBCs as hard disks (26).

Submitted August 27, 2008, and accepted for publication January 8, 2009.

*Correspondence: klaus@liai.org

Editor: Richard E. Waugh.

0006-3495/09/05/4249/11 $2.00

doi: 10.1016/j.bpj.2009.01.060

Additionally, a few advanced computational approaches have been implemented for non-Newtonian leukocyte adhesion analysis (27,28). The Artoli study (27) used a mesoscopic lattice Boltzmann flow solver for shear thinning fluids to describe the dynamics of leukocyte clusters. The Das study (28) modeled non-Newtonian Casson fluid flow of blood in small venules.

The shear stress acting on an adherent leukocyte produces a peeling tension that is transmitted to molecular bonds through the plasma membrane and the cortical cytoskeleton (29). Shear-induced leukocyte rolling has previously been described as a peeling process (30,31), where the energy required to separate the leukocyte from the endothelium is supplied from luminal shear forces through the peeling tension (11). The peeling edge's adhesion energy density, ψ, can be calculated according to

$$\psi = T(1 - \cos\theta), \tag{1}$$

where θ is the angle between the trailing leukocyte edge and endothelial surface and the peeling tension, T, is the integral of the shear stress, τ_s, acting on each membrane element along the free circumference of the adherent cell. Experimentally, the simplest fluid force calculation is to multiply the shear-exposed surface area of the leukocyte with an estimated wall shear stress (11), which is generally based on a Newtonian assumption. However, this simple Newtonian approximation underestimates the wall shear stress by as much as 80% (16,32). In addition, CFD studies have demonstrated that the shear stress acting on an adherent leukocyte is nonuniform and increased relative to wall shear stress (7,27). Experimentally, local shear stress can be calculated from local fluid velocity measurements according to

$$\tau = \mu\frac{\delta v}{\delta r}, \tag{2}$$

where μ is the fluid viscosity, v is the fluid velocity, and the differential is the shear rate, γ, in the radial direction. A linear shear field is a reasonable assumption as long as δr is small, preferably <1 μm, and the measurement is made within the plasma layer. High resolution velocity and position measurements are therefore useful in determining the shear field around an adherent leukocyte.

Our study was designed to obtain a better estimate of the adhesive force and peeling tension acting on an adherent leukocyte through high resolution in vivo measurements of local fluid velocities. To this end, we conducted in vivo microparticle tracking velocimetry (μ-PTV) experiments in venules of the mouse cremaster muscle around hemodynamically isolated adherent leukocytes. Previous velocity measurements have been attempted using a low-resolution particle image velocimetry (PIV) technique in a media-perfused in vitro flow chamber system (33) and in vivo with spinning-disk confocal microscopy in venules from tumor necrosis factor-alpha treated mice (34). Leyton-Mange et al. used a 3.5 × 2.3 μm (width × height) resolution μ-PIV system and found that adhered Jurkat cells experienced a peak shear rate equal to 2–2.5 times the wall shear rate (33). Using a spinning-disk confocal microscope with a 1 μm optical-axis focal depth, King et al. (34) imaged streaks of fluorescent particles in mouse cremaster microvessels. A minimum velocity was obtained for each particle by measuring the streak length and dividing by the illumination time. No force or leukocyte shear stress measurements were reported (34). Here, we report fluid velocities determined in venules in vivo at a sufficiently high resolution and density to measure, for the first time, to our knowledge, the shear stress distribution along an adherent leukocyte. Transgenic mice and monoclonal antibodies enabled the isolated observation of single adherent leukocytes. Velocity measurements across the entire vessel were used to reconstruct cross-sectional velocity profiles upstream and downstream of each adherent leukocyte.

METHODS

Microsphere preparation

Fluoresbrite YG polystyrene microspheres (0.47 ± 0.012 μm diameter; Polysciences, Warrington, PA) were washed twice in 1% bovine serum albumin (BSA, 97% pure; Sigma-Aldrich, St. Louis, MO) and sonicated with an Ultrasonic Cleaner (Fisher Scientific, Pittsburgh, PA) for 10 min to prevent nonspecific adhesion and to disrupt microsphere clusters. No significant population of microsphere aggregates was detected with a Nicomp Submicron Particle Sizer (model 370, Particle Sizing Systems, Santa Barbara, CA; data not shown). Microspheres were suspended in saline to a final concentration of 9×10^9 microspheres/ml.

Intravital microscopy

All animal experiments were conducted under a protocol approved by the University of Virginia Institutional Animal Care and Use Committee (protocol number 2474). Male mice whose neutrophils and monocytes express green fluorescent protein (GFP) (35) were anesthetized with an intraperitoneal injection of ketamine hydrochloride (125 mg/kg; Sanofi Winthrop Pharmaceuticals, New York, NY), atropine sulfate (0.025 mg/kg; Fujisawa, Deerfield, IL), and xylazine (12.5 mg/kg; Phonix Scientific, St. Joseph, MO) and placed on a 37°C heating pad. The trachea, left carotid artery, and left jugular vein were cannulated using polyethylene tubing (Becton Dickinson, Franklin Lakes, NJ), sizes 90, 10, and 10, respectively. The trachea cannulation maintained an open airway whereas the carotid and jugular cannulations allowed for infusion of microspheres, supplemental anesthesia, and P-Selectin antibody Rb40.34 (36). The cremaster muscle was exteriorized, prepared as in (37,38), and pinned to a custom built microscope stage under the continuous flow of body temperature (37°C) bicarbonate-buffered saline (131.9 mM NaCl, 18 mM $NaHCO_3$, 4.7 mM KCl, 2.0 mM $CaCl_2$, and 1.2 mM $MgCl_2$) equilibrated with 5% CO_2 in N_2. Care was taken to limit damage to the cremaster tissue during exteriorization. Surgical trauma results in spontaneous P-selectin dependent leukocyte rolling and adhesion in this model (39). Post-capillary venules were viewed with transillumination (Axioskop intravital microscope, Carl Zeiss, Thornwood, NY) and a saline immersion 40x / 0.75NA or 63x / 0.9NA objective. An adherent leukocyte within a straight unbranched venule was located. Leukocyte rolling, which could interfere with local hemodynamics, was inhibited by multiple injections of 3.75 μg Rb40.34 at 30 s intervals, given until less than one rolling leukocyte passed the adhered cell every 15 seconds. Analysis of additional adherent leukocytes within the same mouse rarely required additional Rb40.34.

Data acquisition

Digital image recordings were captured with a Sensicam QE (Cooke Corporation, Romulus, MI) camera controlled by a dual-core Pentium IV computer with 4 GB RAM, and three 15,000 RPM SAS hard drives in RAID-0 configuration (Dell Computers, Round Rock, TX). This custom computer configuration, with large memory and fast hard drive write speed, allows high-resolution full-field continuous digital recording for 35 s at 10 frames per second. The microscope focus was adjusted to obtain the sharpest leukocyte edges possible. The camera was rotated to align the venule horizontally on the CCD and a region of interest was chosen to exclude tissue >5 μm outside the venule. This procedure enabled recordings at 20–25 frames per second. The camera's exposure-out signal was used to trigger a dual-strobe Xenon lamp with adjustable delay (0.1–99 ms) between the first and second 20-μs duration light pulses (Rapp-OptoElectronic; Hamburg, Germany). Thirty-μL injections of the fluorescent microsphere suspension preceded image acquisition by 10–20 s; 20–30 mixed epi-fluorescence/brightfield frames were collected at the beginning of each recording followed by 600–800 epi-illumination-only frames. Resultant epi-illumination-only frames contained images of microspheres as well as the fluorescent leukocyte. The high propensity for adherent leukocytes to become dislodged, transmigrate, return to a rolling state, or for additional nearby adhesion events to occur required that all data acquisition occur within a 3–5 min time window after locating a stationary leukocyte. On average only five recordings could be collected per mouse with an average of four mice required to obtain a recording of high enough quality (total: 1 recording in 20) for shear stress determination.

Image analysis

Data recordings were analyzed using a custom built (MATLAB, The MathWorks, Natick, MA) semi-automated image analysis graphical user interface (40) which integrates automated bead-pair detection algorithms, a manual correction interface and various analysis tools into a nonprogramming interface. Microsphere centers were determined with two-dimensional Gaussian fitting. Simulations have shown this method to have a better than 10 nm accuracy (41) at the signal/noise ratios exhibited in our imaging system. Assuming a circularly symmetric one-dimensional Gaussian point-spread-function, a bead-blurriness algorithm rejects out-of-focus microsphere images. Testing with training data verified the accuracy of the rejection algorithm. An experienced μ-PTV experimenter scored microsphere images as in-focus or out-of-focus. Applied to the same training dataset, the automatic rejection algorithm correctly accepts 96% of in-focus while rejecting 81% of out-of-focus microsphere images (40). In its entirety, the automatic bead-pair detection algorithm correctly identifies 67% of bead pairs. Four percent of automatically identified bead pairs were the result of erroneous detections. All automatic results were reviewed by an experienced μ-PTV user and errors or omissions were corrected. Vessel borders were identified from brightfield images as previously described (32). Leukocyte borders were identified from epi-illumination images as the transition pixel between the bright leukocyte and dark lumen.

Data analysis

Local fluid velocities were calculated from the measured spatial separation of imaged bead pairs and known delay between the dual-flash illuminations.

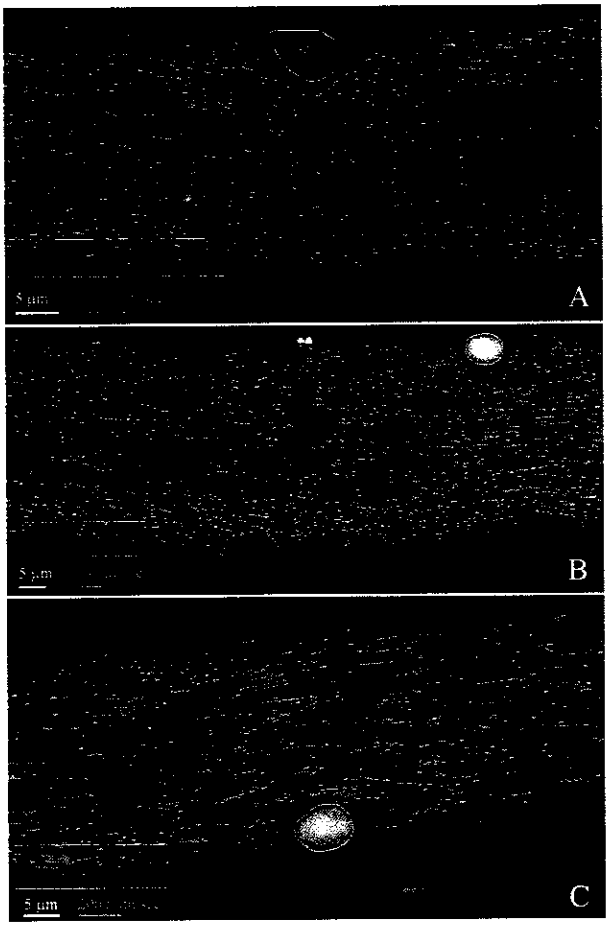

FIGURE 1 Measured μ-PTV velocity field (*arrows*) superimposed on representative intravital fluorescence image of adhered eGFP-expressing leukocyte (*encircled*) for experiments A (*A*), B (*B*), and C (*C*). Vessel walls are highlighted by horizontal lines. μ-PTV velocity data obtained by measuring the distance between bead instances and dividing by the known temporal strobe separation. Arrows represent individual velocity measurements with length and direction proportional to measured velocity vector. Wall shear rate was calculated from data inside the white box. Leukocyte and vessel borders were manually drawn. Velocity and length scale lower right.

Near-wall micro-fluidics results in microspheres traveling slower than the underlying fluid. The analytic results of (10) were used to correct for this effect. An adherent leukocyte disrupts blood flow for a small distance up- and downstream. This distance, L_{d2}, was calculated based on the leukocyte, r_l, and vessel radius, R, according to (42):

TABLE 1 Geometric measurements and number of bead pairs for experiments A, B, and C

	D (μm)	L_U (μm)	L_D (μm)	Ld_2 (μm)	Flow (nl/s)	v_{max} (μm/s)	WBC_H (μm)	WBC_L (μm)	No. BP	No. BP_w	No. BP_L	h_{esl} (μm)
A	29	37	60	21	0.30	760	5.7	8.7	885	14	27	0.41
B	39	102	55	23	0.47	721	5.9	7.0	1970	11	22	0.19
C	34	79	54	24	1.10	2485	6.5	8.0	643	16	12	0.39

Column headers, from left-to-right: vessel diameter, upstream length to closest hemodynamic disturbance, downstream length to closest hemodynamic disturbance, calculated length of disturbed flow based on Eq. 3, bulk fluid flow (see text for details), maximum measured velocity, leukocyte height, leukocyte length, number of in focus bead pairs, number of bead pairs used for linear shear rate calculation, number of bead pairs within 2 μm of the adherent leukocyte, and endothelial surface layer thickness.

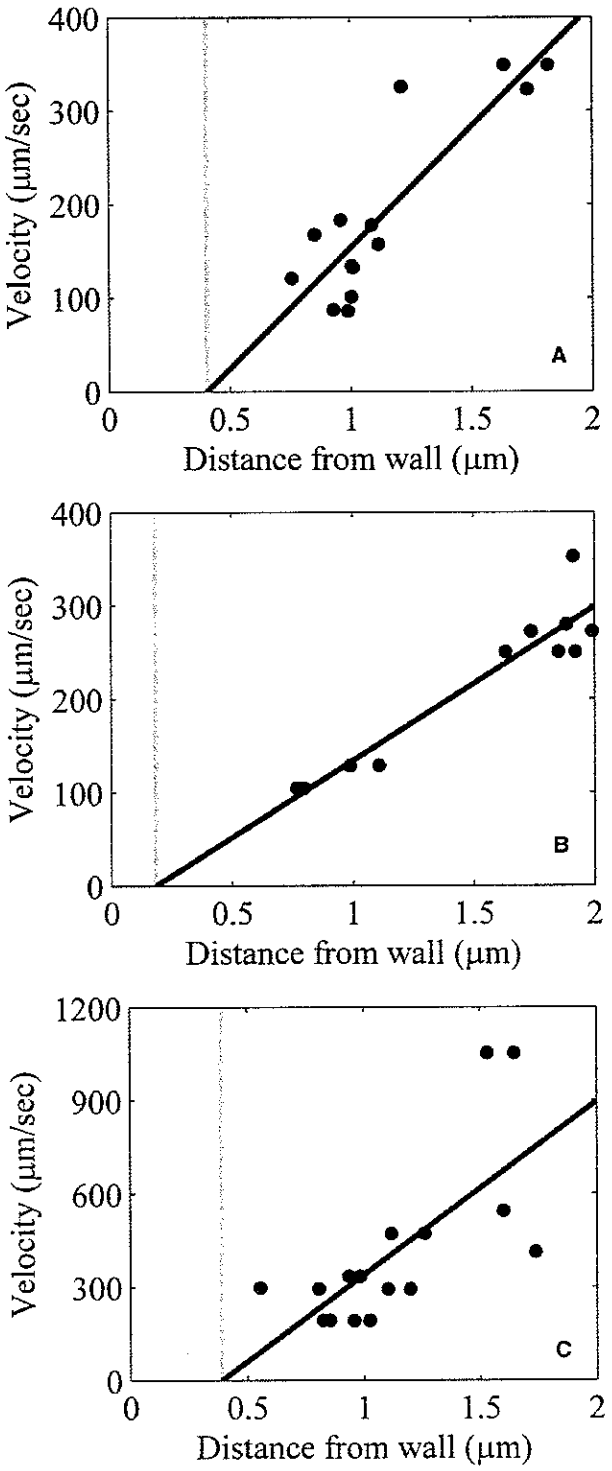

FIGURE 2 Translational velocities of μ-PTV data from boxed areas in Fig. 1 within 2 μm of the vessel wall for experiments A (*A*), B (*B*) and C (*C*). Linear fits of these data (*solid black lines*, $R^2 = 0.85$, 0.89, 0.49, respectively) show a negative velocity intercept at the vessel wall indicating the presence of an endothelial surface layer (32), dashed black line, with thickness 0.41, 0.19, and 0.39 μm, respectively. Wall shear rate γ_w calculated from the slope of the linear fit as 259, 165, and 557 s^{-1}, respectively.

$$\frac{L_d}{2} = L_{d2} = 2R\left(-0.12 + 6.22(r_l/R) - 11.69(r_l/R)^2 + 11.04(r_l/R)^3 - 4.02(r_l/R)^4\right). \quad (3)$$

Hemodynamic interactions induce a cell-free zone near the vessel wall (43) permitting a Newtonian assumption and resulting in a locally linear velocity profile. Wall shear rates were determined from linear fits of velocity data within 2-μm of the vessel wall (16). The microvascular endothelium is covered with an endothelial surface layer (ESL) (44), the thickness of which was determined as the radial distance of the zero-velocity intercept (32). Similarly, a shear rate measurement was calculated for each microsphere image within 2 μm of the leukocyte by dividing the microsphere velocity by its perpendicular distance to the luminal cell surface.

Centerline velocity profiles were determined from fluid velocity measurements in a 15 μm vessel segment upstream of the adherent leukocyte combined with measurements from a similarly sized segment downstream of the cell. Out-of-focus bead pairs were rejected using an automated algorithm (19,40) and a hydrodynamic-based monotonic filter algorithm (16). Reneman et al. proposed the following function form for venular velocity profiles, which was fit to the filtered data (45):

$$v(r) = v_{max}\left(1 - \left|a\frac{r}{R} + b\right|^k\right). \quad (4)$$

Variables v_{max}, a, b, and k are model fitting parameters. The ESL thickness, determined as above, was subtracted from vessel diameters, as measured in brightfield images, to obtain the hydrodynamically relevant vessel radius. Differential of this profile, evaluated at the vessel wall, provides a second independent measure of the wall shear rate. Fluid flow rate was determined by integration of the velocity profile.

RESULTS

Local velocities were obtained by analyzing more than 24,000 bead pairs in 69 cremaster venules of 13 lysM-GFP mice. The quality of these recordings was analyzed using the following criteria: 1), straight, unbranched vessel with clearly visible endothelial cells and vessel wall over most of the length of the venule 2), one single adherent leukocyte that did not move more than 1 μm throughout the full recording time of 35 s 3), leukocyte hydrodynamically isolated or further than one vessel diameter from the nearest adherent leukocyte or bifurcation 4), leukocyte adherent to the "side" wall as determined by the alignment of its fluorescent outline with the continuity of the endothelial surface 5), a minimum of 500 in-focus bead pairs successfully detected 6), a minimum of 10 in-focus bead pairs within 2 μm of the adherent leukocyte, and 7), centerline blood flow velocity between 500 and 4000 μm/s. Justification for the separation distance in criteria (3) can be found from modeling experiments (46) which show the hydrodynamic effects of protrusions in low Reynolds number flow extend for ~1 vessel diameter and from the calculated disturbance distance, L_d (Eq. 3). Three of 69 recordings, denoted experiments A, B and C, fulfilled these stringent criteria and were analyzed in detail (Fig. 1). Table 1 lists the geometric and experimental parameters for these experiments.

TABLE 2 Calculated hemodynamic parameters for experiments A, B, and C

	$\gamma_{w\text{-}new}$ (1/s)	$\gamma_{w\text{-}lin}$ (1/s)	$\gamma_{w\text{-}prof}$ (1/s)	$\gamma_{l\text{-}max}$ (1/s)	T_{new} (dyn/cm)	T_{lin} (dyn/cm)	T_{prof} (dyn/cm)	$T_{l\text{-}max}$ (dyn/cm)	$T_{l\text{-}meas}$ (dyn/cm)
A	133	259	169	570	2.30E-03	4.45E-03	2.91E-03	9.80E-03	3.61E-03
B	80	165	89	994	1.39E-03	2.85E-03	1.54E-03	1.72E-02	3.13E-03
C	287	557	355	1996	5.39E-03	10.45E-03	6.66E-03	3.74E-02	7.74E-03

Wall shear rate calculated three ways: using a Newtonian approximation, $\gamma_{w\text{-}new}$, using a linear fit of near wall data, $\gamma_{w\text{-}lin}$, and with a profile fitting method, $\gamma_{w\text{-}prof}$. Maximum measured shear rate on leukocyte surface in forth column, $\gamma_{l\text{-}max}$. Peeling tension calculated from each of these shear rate estimates by multiplication by the measured free-circumference length of the adhered leukocyte: T_{new}, T_{lin}, T_{prof}, and $T_{l\text{-}max}$, respectively. Actual peeling tension as calculated from integration of measured shear stress along the length of the leukocyte mid-plane, $T_{l\text{-}meas}$ (see text for details).

Data for all experiments are available (see the Supporting Material).

The radial probability distribution of detected bead pairs was analyzed for uniformity. This analysis showed uniformity across the vessel center. From there (normalized radial distance $r/R = \pm 0.35$), the probability distribution rises to a peak of detected bead pairs at a normalized radial distance of $r/R = \pm 0.75$, where they are 2.5 times as frequent as in the vessel center. This may reflect radial migration of small microspheres as described previously (47). The probability distribution falls to almost zero probability at the vessel walls, most likely because very slow beads are mostly not resolved into a bead pair, because the strobe delay is too short. Across all three experiments, 1.5% of detected bead pairs were within 1 μm of the vessel wall. In the center, multiple fast microspheres can be difficult to parse into corresponding bead pairs and microspheres appearing near the edge of the field of view will have a greater chance for the corresponding bead pair to be outside of the field of view: i.e., the delay is too long. Also, the microscope depth of focus is not as thick as the vessel center, thus some beads go undetected. Finally, light penetration may be limited in the center of the vessel, mostly because hemoglobin absorbs at the wavelengths used for excitation.

For each venule, wall shear rate, γ_w, was determined from velocity measurements within the boxed regions in Fig. 1 as described in Smith et al. (32). Wall shear stress, τ_w, was calculated using experimentally determined mouse plasma viscosity (1.0 $\pm$ 0.05 cP at 37°C) (24). ESL thickness and wall shear rate determination is illustrated in Fig. 2 for all three experiments, the results of which are listed in Table 2. To confirm this estimate of wall shear rate, we used a second method, based on the full cross-sectional velocity profile (45) as described above. Due to an upstream bifurcation, only velocities from a 10 μm vessel segment in experiment A (compared to 15 μm segments for experiments B and C) were included. Fig. 3 shows the filtered data from experiment B and the resultant well-defined velocity profile.

Shear stresses acting on adherent leukocytes were determined from bead pairs within 2 μm of the cell surface. Close-up images of the near-leukocyte velocity measurements for all three experiments are shown in Fig. 4. For each microsphere position within 2 μm of the leukocyte surface, we calculated the local shear rate acting on the adherent leukocyte, γ_s, and normalized it to the wall shear rate, γ_w. Based on earlier CFD work (48), an angle, θ, was defined between the leukocyte peeling edge, leukocyte center and microsphere position (Fig. 5 *A*, *inset*). Grouping shear rate measurements into similar stress regions, as shown in Fig. 5 *A* (*inset*), we repeated the linear fit analysis to determine shear rate and ESL thickness. The linear fits mostly displayed a near-zero, but positive, velocity intercept with the leukocyte surface, indicating that the thickness of the leukocyte surface layer, if any, was negligible. Fig. 5 *A* shows normalized shear rate as a function of θ from experiments A, B and C; Fig. 5 *B* shows these data binned in increments of 10° and averaged across all three experiments. Peeling tension, T, was calculated by integrating the shear stress around the free leukocyte surface (Table 2). Our integrated tension is compared to the tension calculated by multiplying the free membrane length by i), a traditional Newtonian assumption of wall shear stress, T_{new}, and ii), the actual wall shear stress as measured by a linear fit to μ-PTV, T_{lin} (Table 2). Our data shows that the Newtonian-based calculation underestimates the peeling tension, on average, by 41% and the wall shear stress-based calculation still has an average error of 22%. Based on these measurements, we constructed maps of the surface stresses as seen in Fig. 5, *C–E*. Here, shear data from all three experiments are represented as a color-coded shear rate around a leukocyte, with a shape based on our measured shapes. The normalized shear rates are graphically displayed for each experiment in panels *F–H* of Fig. 5.

Rolling and adherent leukocytes protrude into the vessel lumen causing a deflection of fluid velocity streamlines. As can be seen in Fig. 1, the velocity vectors near the adhered leukocytes are no longer parallel to the vessel walls, but are deflected toward the vessel centerline upstream of, and toward the vessel wall downstream of, the adhered leukocyte. This was systematically analyzed and expressed as a deflection angle Φ defined as,

$$\Phi = \sin^{-1}\left(\frac{\Delta d}{d_{1-2}}\right), \tag{5}$$

where Δd is the change in wall distance between the first and second microsphere positions (4–8 ms apart) and d_{1-2} is the measured bead pair separation distance. Microspheres deflected away from the wall to which the leukocyte is adhered have a negative deflection angle. Unfiltered datasets from all

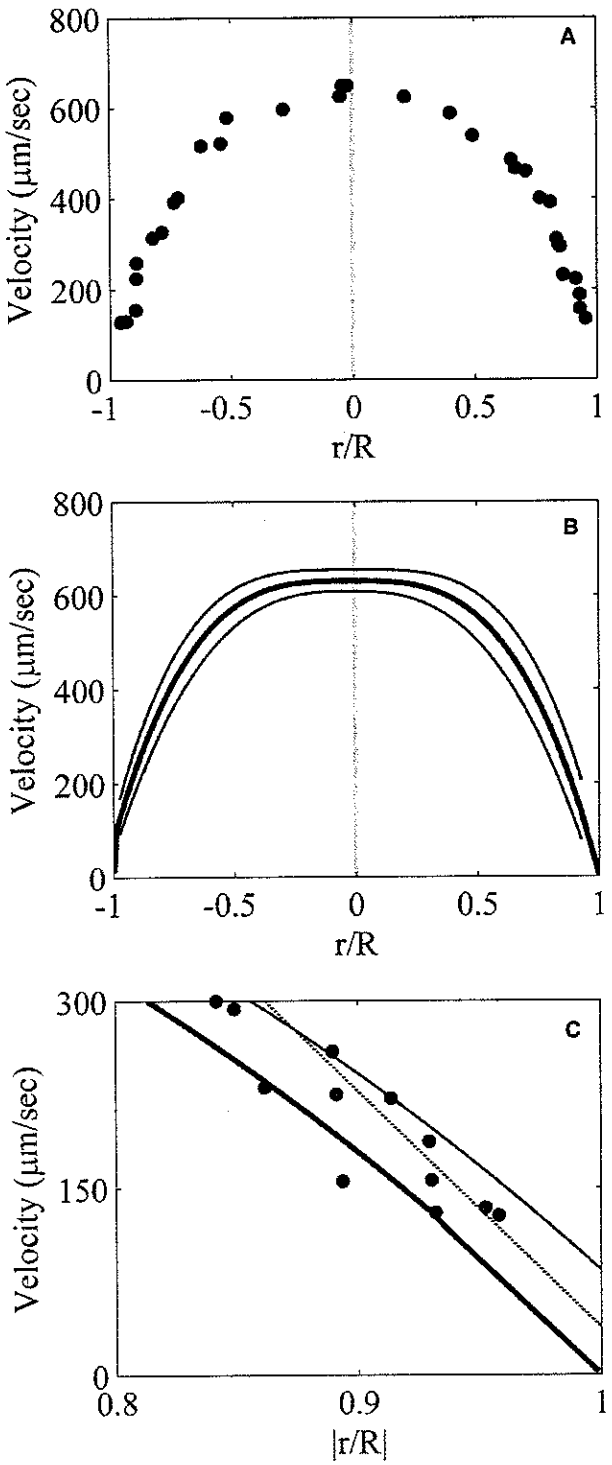

FIGURE 3 (*A*) Velocity measurements remaining after monotonic filtering of μ-PTV experiment B as a function of normalized distance, r/R, from vessel centerline. Data taken from a 15-μm wide segment upstream and downstream of the adherent leukocyte. Vessel radius, R, calculated by the exclusion of the ESL protrusion distance from brightfield measurements of vessel diameter. (*B*) Velocity profiles constructed by fitting μ-PTV data from panel *A* to Eq. 4 (*dark solid line*) with 95% confidence levels (*light solid lines*). Near-wall velocity profile determined by linear fit with closest velocity measurement to ESL-lumen boundary. (*C*) Shear rate comparison between linear- and profile-fitting methods. Data points are velocity measurements from experiment B plotted as absolute normalized distance from the vessel centerline. Shear rate determined from a linear fit of velocity measurements within 2 μm of the wall (*dotted line*). The derivatives of the fitted profile at r/R equal to 1 (*dark solid line*) and -1 (*light solid line*) provide a second measure of wall shear rate.

three experiments (Fig. 6, *A–C*), including only measurements within 4 μm of the leukocyte surface or vessel wall, show a systematic deviation of the velocity-vector angle in the vicinity of the leukocyte. Deflection angles for all three experiments were binned into 2 μm wide vessel cross sections and averaged (Fig. 6 *D*). For comparison, angular deflection of velocity vectors measured within 4 μm of the wall opposite the adhered leukocyte (Fig. 6 *E*) were obtained. An asymmetric pattern of velocity vector angles upstream and downstream of the center of the leukocyte can be seen for near-leukocyte measurements. Upstream microspheres, on average, become increasingly deflected toward the vessel center at a rate of 2.07°/μm ($R^2 = 0.83$) whereas downstream microspheres return to zero deflection at a rate of 1.17°/μm ($R^2 = 0.66$). Microspheres located over the leukocyte reverse their deflection (become increasingly deflected toward the wall to which the leukocyte is adhered) at a rate of 2.88°/μm ($R^2 = 0.87$). No such trend is found among the angular deflection of control velocity measurements within 4 μm of the wall opposite the adherent leukocyte.

DISCUSSION

In vivo hemodynamics in the vicinity of adherent leukocytes was characterized from local velocity measurements using a particle tracking technique: μ-PTV. The effective depth of field (DOF) for these measurements was limited by a novel blurriness rejection algorithm (40) which, when compared to a human observer, demonstrated a >90% success rate for rejection and acceptance of out-of-focus and in-focus particle images, respectively. In-plane error of automated particle localization is estimated to be <0.1 pixels (10 nm) (41), a precision greater than that possible by manual tracking (49). Measured fluid velocities around adherent leukocytes showed an average peak shear rate of four times the wall shear rate. Integration of the fluid shear stress along the shear-exposed cell membrane suggests an average peeling tension of 4.8×10^{-3} dyne/cm. Protrusion of adhered and rolling leukocytes into the vessel lumen deflected the fluid streamlines toward the vessel axis. Deflection was found to be more severe on the leukocyte's upstream edge when compared to deflection at its downstream edge.

The largest source of error in particle image or tracking velocimetry experiments is positional uncertainty along the optical axis. Traditional PIV experiments utilize planar

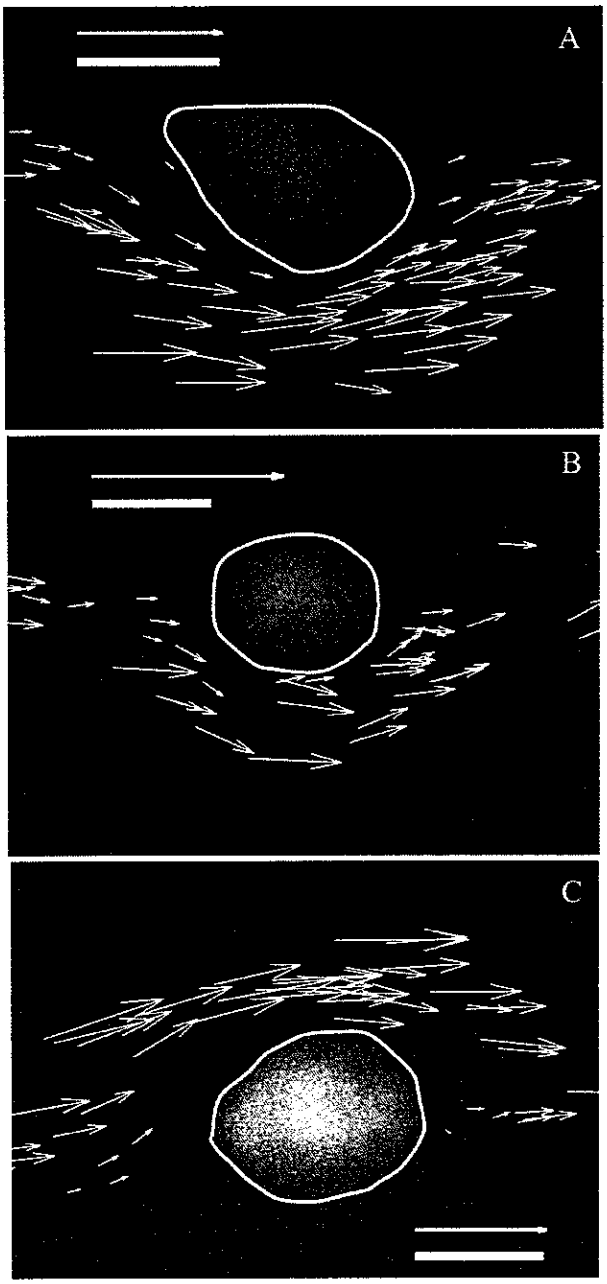

FIGURE 4 Near-leukocyte velocity measurements from experiments A (*A*), B (*B*), and C (*C*) and within 4 μm of the leukocyte or vessel wall (*white arrows*), as in Fig. 1. Leukocyte and vessel borders shown as solid and dotted lines, respectively. Solid scale bar is 5 μm, arrow scale bar is 1000 μm/s (*A* and *B*) or 2000 μm/s (*C*).

illumination to minimize this shortcoming; however, this type of lighting is not possible for microscopic in vivo experiments. Alternatively, statistically based PIV algorithms can remove, or at least measure, the effects from out-of-focus particles (50). These statistical techniques are not suitable for the single-microsphere measurements used in PTV where an in-focus or out-of-focus decision must be made from a single microsphere image. A hydrodynamics-based filter has been developed for μ-PTV which limits the DOF to the midsagittal plane (51). This method was used in this study for velocity profile determination; however, it is not applicable for near-leukocyte measurements, where the velocity profile is not axially symmetric. We have limited the DOF by rejecting blurred microsphere images but cannot exclude the possibility of erroneous measurements from out-of-plane microspheres.

The nonuniformity of the radial distribution of detected bead pairs may indicate a migration of microsphere toward particular radial positions, but the confidence in this conclusion is limited because a bead pair may go undetected in the vessel center and near the vessel walls for the reasons given above. An excess of measurements in a given location does not really affect the validity of our measurements. Only the velocity profile and angular deflection measurements are based on a statistical analysis of multiple measurements. In terms of the velocity profile, the hydrodynamics-based filter ensures that only the fastest detected microspheres at a given radial location are utilized. The higher distribution of measurements near the normalized radial position (r/R) of 0.75 would tend to bias the profile fitting process to more accurately represent this portion of the profile. Since the velocity profile becomes steeper closer to the vessel wall, the effect of this bias would be to underestimate the wall shear rate determined using this profile fitting method. Since relatively fewer measurements are included from near the center of the vessel, the nonuniform distribution of measurements also has the effect of biasing the angular deflection data toward higher rates of deflection.

Deflection of velocity vectors away from parallel with the vessel centerline provides a measurement of the extent to which rolling and adherent leukocytes affect local hemodynamics. Our measurements show that an adherent leukocyte deflects streamlines away from (toward) the wall to which it is adhered to at least one vessel radius upstream (downstream) of the leukocyte's center. This assessment is consistent with CFD models which show the extent of the hemodynamic influence to extend one vessel diameter up- and downstream of the adherent leukocyte (42). Our minimum disturbance distances are also consistent with a calculated length of disturbance from an empirically derived equation (52) (Eq. 3, Table 1). The calculated values are greater than our minimum estimation of one vessel radius.

Streamline deflection has previously been measured experimentally using a technique similar to μ-PTV (34). In this study, continuous illumination provided image streaks as microspheres flowed across the field of view. The angular deflection was reported in this study as the absolute value of the radially directed microsphere motion. In the current study, we have reported the average of the actual angular deflection to determine how velocity streamlines change from a negative (toward the vessel axis) to positive (toward

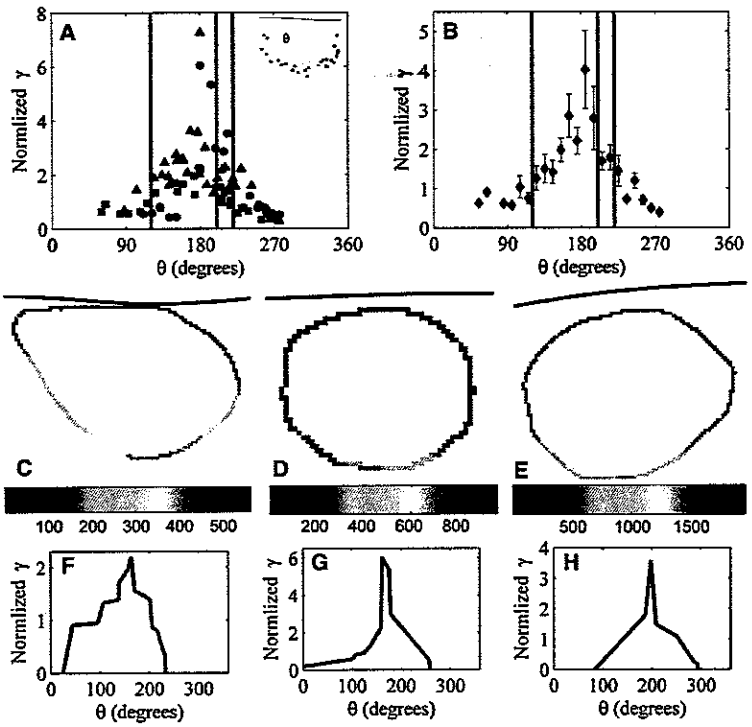

FIGURE 5 (*A, inset*) Example subdivision, from experiment A, of μ-PTV data into four distinct regions around the adherent leukocyte. Angular position, θ, determined as the angle between the lines formed by the leukocyte center to trailing edge and leukocyte center to bead image. Velocity measurements divided into four regions: 0–120° (*circles*), 120–200° (*triangles*), 200–220° (*squares*), and 220–360° (*diamonds*). Black lines denote boundaries between regions. (*A*) Normalized shear stress acting on the surface of the adherent leukocyte for μ-PTV data within 2 μm of leukocyte from experiments A (*open triangles*), B (*circles*), and C (*solid triangles*). Dotted lines denote boundaries between angular regions. (*B*) Data from center-left panel averaged into 10 degree bins. (*Center panels*) Map of shear rate on the leukocyte surface for experiments A (*C*), B (*D*), and C (*E*). Wall location shown as black line. (*bottom panels*) Normalized shear rate data for experiment A (*F*), B (*G*), and C (*H*).

the vessel wall) slope as they move around an adherent leukocyte.

Wall shear stress was determined with two separate methods: a linear fit (32) and full-profile determination (45) (Eq. 4). Results from these methods are compared to the calculated wall shear stress using a traditional Newtonian assumption (Table 2). High spatial resolution μ-PTV measurements allow determination of the fluid velocity within the cell-free layer where the velocity profile is near-linear and the shear rate is constant, as previously described (32). Estimation with lower resolution techniques, such as PIV (33) or PTV with larger particles (22), cause an averaging of velocities in the radial direction and cannot accurately measure very-near wall velocities, where the shear rate is highest. Thus, these techniques typically underestimate the wall shear rate (16). The full-profile determination method used here was originally derived from lower resolution velocity measurements (22). The low-resolution measurements always display a positive velocity at the fluid-wall interface. The profile fitting method was updated to a linear profile from the velocity measurement nearest the wall to zero velocity at the wall (45). Assessment of the wall shear rate based on a single velocity measurement provides little robustness to the measurement error. Using the same profile definition with higher resolution velocity measurements should provide more accurate wall shear rate determination.

In this study, the thickness of the endothelial surface layer was subtracted from the vessel radius before profile fitting, resulting in improved accuracy of the shear rate estimate. ESL thicknesses (Table 1) were found to be consistent with the previous measurements (32,53). Wall shear rate was found to be higher with the linear fit measure. Only near-wall fluid velocities determine the wall shear rate; however, the empirically determined profile fitting method must be optimized with respect to both near-wall and near-center velocity measurements. We conclude that the linear fit method provides a more accurate measure of the actual wall shear rate.

The fluid shear rate was measured along the length of the shear-exposed leukocyte cell membrane. PIV measurements have previously been made around an adherent Jurkat cell in a side-view flow chamber (33). These cells (22 μm diameter) are larger than natural leukocytes (8 μm diameter) and were reportedly chosen to produce a measurable flow disturbance. The large cross-sectional area of this flow chamber required cell isolation and perfusion with cell media reducing the experiment's physiologic relevance but enabling a Newtonian assumption for corresponding CFD modeling. Leyton-Mange et al. used a 3.5 μm resolution PIV method, almost an order of magnitude lower resolution than the μ-PTV method presented in this study (0.47 μm resolution). The peak shear stress, of 2.5 times the wall shear stress, reported by Leyton-Mange et al. is consistent with their own two-dimensional and three-dimensional modeling work (33,54,55) as well as CFD modeling of leukocytes adhered in a parallel plate flow chamber under Newtonian flow reported by other groups (13,56). Similar results were

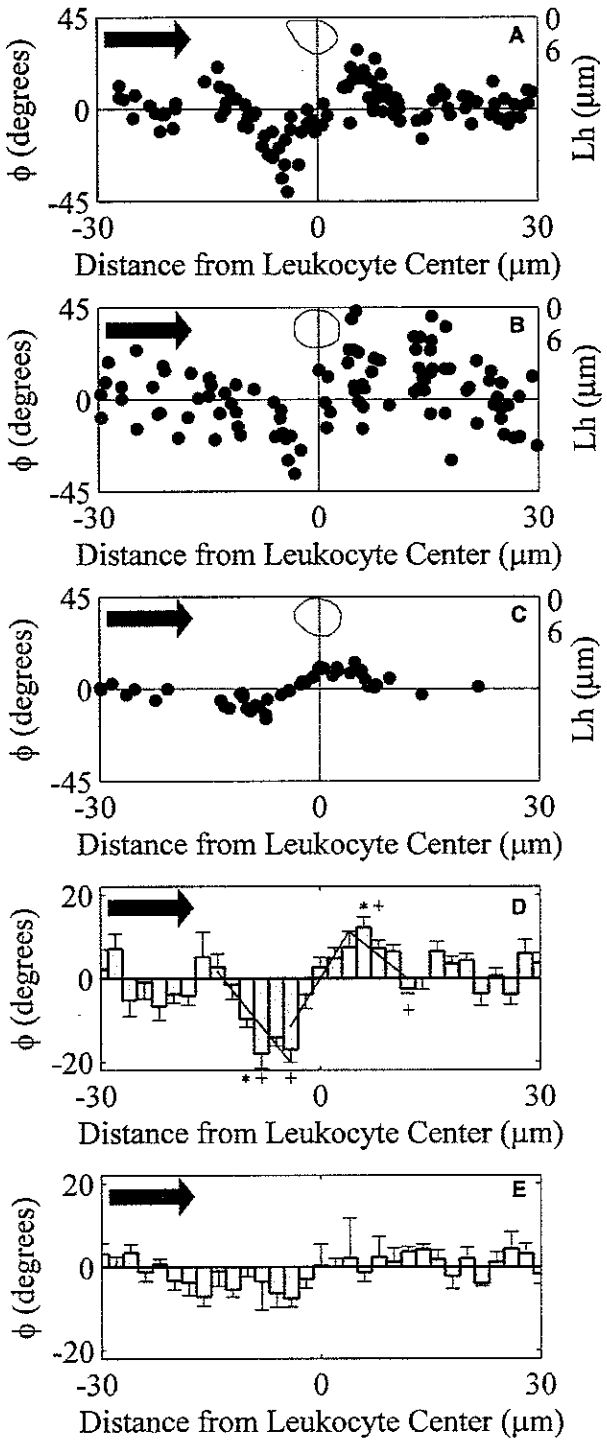

FIGURE 6 (*A–C*) Angular deflection, Φ, of imaged bead pairs from experiment A (*A*), experiment B (*B*) and experiment C (*C*), left axis, as calculated according to Eq. 5. Negative deflection angles are away from the vessel wall to which the leukocyte is adhered. Leukocyte shape shown as a reference (*thin solid line*), with height (*Lh*) on right axis. Arrow shows direction of blood flow. (*D and E*) Angular deflection of imaged bead pairs from all three experiments averaged into 2 μm sized bins. Error bars denote standard error. (*D*) Only data within 4 μm of leukocyte or vessel wall to which leukocyte is adhered are included. Linear fits of bin averages from an upstream region (from −15 to −3 μm), leukocyte region (from −5 to 5 μm) and downstream region (3–15 μm) are shown as sloped lines and have slopes −2.07, 2.88, and −1.17 degrees/μm, respectively ($R^2 = 0.83$, 0.87, 0.66). Asterisks and crosses denote bin averages which are significantly different ($p < 0.01$ and $p < 0.05$, respectively) from opposing wall data. (*E*) Only data within 4 μm of vessel wall opposite the wall to which the leukocyte is adhered are included.

obtained from cylindrical tube modeling for a low leukocyte radius/tube radius ratio (7,42,46). This peak shear rate value from Newtonian fluid flow is only 50–75% of our measured value in vivo, suggesting that higher peak shear rates in vivo may be reached because of the very steep velocity profile in the near-wall plasma layer. Two CFD studies of leukocyte adhesion, using two different modeling frameworks, have incorporated the non-Newtonian effects of blood flow. One study reports that the peak shear stress on the leukocyte surface is always greater than the wall shear stress but does not quantify how much greater (27). The second non-Newtonian study reports a maximum shear stress that is 4.5 times the wall shear stress assuming a 1.8 μm cell-free layer thickness and leukocyte radius to vessel radius of 0.24 (28). This result is remarkably similar to our measured average peak shear stress of four times the wall shear stress.

Cell deformation has a large effect on the shear stresses experienced by an adherent cell. A deformed cell is flatter and occludes less of the vessel lumen, thus reducing the peak shear stress on the cell surfaces; however, the deformed cell also elongates exposing a greater surface area to fluid forces. CFD studies have shown that for all but the largest deformations, the reduction in cell height is of greater importance than the increase in cell length and the total force decreases by a modest 10–20% (7,54). The shape of the shear stress distribution along the leukocyte length is a major determinant of the total fluid-imparted shear stress. For a spherical cell under Newtonian flow, the shear stress distribution is symmetric about the cell center. Of the three experiments presented in this study, only the cell in experiment B had a nearly spherical shape, but the measured shear stress distribution was still asymmetrical, another potential influence of non-Newtonian effects. Our shear stress distribution agrees well with the calculated distribution from a CFD study that modeled the leukocyte from the measured cell shape found in experiment A (M. Sugihara-Seki and H. O-tani, Kansai University, personal communication, 2008).

A peeling tension was calculated as the force per unit length of cell membrane in the z-direction. The peeling tension is resisted by molecular bonds and can be related to the energy density of the cellular adhesion (Eq. 1) (11). Damiano et al. reported adhesion energy density values that are an order of magnitude greater than our measured values. Their energy density calculation was dependent on an estimated peeling tension. The peeling tension was calculated from the average shear stress on the leukocyte surface

which, in turn, was estimated from CFD modeling (13) as three times the wall shear rate. Our measurements have directly measured the peeling tension (Table 2) and energy density. Our measurements show that although the peak shear rate on the leukocyte surface is indeed higher than the average wall shear rate, the average shear rate on the leukocyte surface is much lower than the assumption of Damiano et al. resulting in a lower adhesion density than previously estimated. Our measurements actually agree with an analytically derived result of 3.4×10^{-3} dyne/cm (57) and show that the peeling tension acting on the leukocyte surface is similar to that derived from multiplying wall shear rate with free arc length.

These results are not solely limited to adherent cells. Fluid forces are determined by the velocity differential at the fluid-wall interface (Eq. 2). Adaptation of these results for rolling leukocytes would require a slight reduction of the measured fluid velocities by the velocity of the rolling cell, which is on the order of 10μm/s (2). The peeling tension and adhesion energy density on these cells would be quite similar to the measured peeling tension on adherent cells since the fluid-cell velocity difference is much higher than the rolling velocity. The slowest (fastest) fluid velocity measurements around an adhered leukocyte were on the order of 100 μm/s (1000 μm/s) which would correspond to a 10% (1%) peeling tension difference between rolling and adherent cells.

Significant magnitude differences exist between our measured shear rates and those calculated from CFD models which have assumed a Newtonian perfusate; however, CFD models which include non-Newtonian effects agree well with our measurements. This underscores the need to account for the effect of RBC aggregation and lateral migration, resultant profile blunting, and formation of the near-wall cell-free layer. This also suggests that the commonly used Goldman approximation (10) for the fluid force exerted on a sphere near a planar wall underestimates the actual shear force acting on adherent and rolling leukocytes under whole blood shear flow, which is consistent with previous CFD models (7,14).

SUPPORTING MATERIAL

Two tables are available at http://www.biophysj.org/biophysj/supplemental/S0006-3495(09)006705.

REFERENCES

1. Tozeren, A., and K. Ley. 1992. How do selectins mediate leukocyte rolling in venules? *Biophys. J.* 63:700–709.
2. Atherton, A., and G. V. R. Born. 1973. Relationship between the velocity of rolling granulocytes and that of the blood flow in venules. *J. Physiol.* 233:157–165.
3. Lawrence, M. B., and T. A. Springer. 1991. Leukocytes roll on a selectin at physiologic flow rates: Distinction from and prerequisite for adhesion through integrins. *Cell.* 65:859–873.
4. Caputo, K. E., D. Lee, M. R. King, and D. A. Hammer. 2007. Adhesive dynamics simulations of the shear threshold effect for leukocytes. *Biophys. J.* 92:787–797.
5. Hammer, D. A., and S. M. Apte. 1992. Simulation of cell rolling and adhesion on surfaces in shear flow: general results and analysis of selectin-mediated neutrophil adhesion. *Biophys. J.* 63:35–57.
6. Reference deleted in proof.
7. Sugihara-Seki, M. 2000. Flow around cells adhered to a microvessel wall. I. Fluid stresses and forces acting on the cells. *Biorheology.* 37:341–359.
8. Khismatullin, D. B., and G. A. Truskey. 2005. Three-dimensional numerical simulation of receptor-mediated leukocyte adhesion to surfaces: Effects of cell deformability and viscoelasticity. *Phys. Fluids.* 17:031505.
9. Jadhav, S., C. D. Eggleton, and K. Konstantopoulos. 2005. A 3-D Computational Model Predicts that Cell Deformation Affects Selectin-Mediated Leukocyte Rolling. *Biophys. J.* 88:96–104.
10. Goldman, A., R. Cox, and H. Brenner. 1967. Slow viscous motion of a sphere parallel to a plane wall—II Couette flow. *Chem. Eng. Sci.* 22:653–660.
11. Damiano, E. R., J. Westheider, A. Tozeren, and K. Ley. 1996. Variation in the velocity, deformation, and adhesion energy density of leukocytes rolling within venules. *Circ. Res.* 79:1122–1130.
12. House, S. D., and H. H. Lipowsky. 1988. In vivo determination of the force of leukocyte-endothelium adhesion in the mesenteric microvasculature of the cat. *Circ. Res.* 63:658–668.
13. Brooks, S., and A. Tozeren. 1996. Flow past an array of cells that are adherent to the bottom plate of a channel. *Comput. Fluids.* 25:741–757.
14. Pozrikidis, C. 2000. Effect of pressure gradient on viscous shear flow past an axisymmetric depression or protuberance on a plane wall. *Comput. Fluids.* 29:617–637.
15. Sugihara-Seki, M. 2001. Flow around cells adhered to a microvessel wall II: Comparison to flow around adherent cells in channel flow. *Biorheology.* 38:3–13.
16. Long, D. S., M. L. Smith, A. R. Pries, K. Ley, and E. R. Damiano. 2004. Microviscometry reveals reduced blood viscosity and altered shear rate and shear stress profiles in microvessels after hemodilution. *Proc. Natl. Acad. Sci. USA.* 101:10060–10065.
17. Cao, J., B. Donell, D. R. Deaver, M. B. Lawrence, and C. Dong. 1998. In vitro side-view imaging technique and analysis of human T-leukemic cell adhesion to ICAM-1 in shear flow. *Microvasc. Res.* 55:124–137.
18. Lipowsky, H. H. 2005. Microvascular rheology and hemodynamics. *Microcirculation.* 12:5–15.
19. Rychak, J. J., B. Li, S. T. Acton, A. Leppanen, R. D. Cummings, et al. 2006. Selectin ligands promote ultrasound contrast agent adhesion under shear flow. *Mol. Pharm.* 3:516–524.
20. Chien, S. 1987. Red cell deformability and its relevance to blood flow. *Annu. Rev. Physiol.* 49:177–192.
21. Schmid-Schonbein, G. W. 1999. Biomechanics of microcirculatory blood perfusion. *Annu. Rev. Biomed. Eng.* 1:73–102.
22. Tangelder, G. J., D. W. Slaaf, T. Arts, and R. S. Reneman. 1988. Wall shear rate in arterioles in vivo: least estimates from platelet velocity profiles. *Am. J. Physiol. Heart Circ. Physiol.* 254:H1059–H1064.
23. Bishop, J. J., A. S. Popel, M. Intaglietta, and P. C. Johnson. 2001. Effects of erythrocyte aggregation and venous network geometry on red blood cell axial migration. *Am. J. Physiol. Heart Circ. Physiol.* 281:H939–H950.
24. Smith, M. L., M. J. Smith, M. B. Lawrence, and K. Ley. 2002. Viscosity-independent velocity of neutrophils rolling on p-selectin in vitro or in vivo. *Microcirculation.* 9:523–536.
25. Soutani, M., Y. Suzuki, N. Tateishi, and N. Maeda. 1995. Quantitative evaluation of flow dynamics of erythrocytes in microvessels: influence of erythrocyte aggregation. *Am. J. Physiol.* 268:H1959–H1965.
26. Chapman, G. B., and G. R. Cokelet. 1996. Model studies of leukocyte-endothelium-blood interactions. I. The fluid flow drag force on the adherent leukocyte. *Biorheology.* 33:119–138.
27. Artoli, A. M., A. Sequeira, A. S. Silva-Herdade, and C. Saldanha. 2007. Leukocytes rolling and recruitment by endothelial cells: Hemorheological experiments and numerical simulations. *J. Biomech.* 40:3493–3502.

28. Das, B., P. C. Johnson, and A. S. Popel. 2000. Computational fluid dynamic studies of leukocyte adhesion effects on non-Newtonian blood flow through microvessels. *Biorheology*. 37:239–258.

29. Tozeren, A., L. H. Mackie, M. B. Lawrence, P.-Y. Chan, M. L. Dustin, et al. 1992. Micromanipulation of adhesion of phorbol 12-myristate-13-acetate stimulated T-lymphocytes to planar membranes containing Intercellular Adhesion Molecule-1. *Biophys. J.* 63:247–258.

30. Bell, G. I., M. Dembo, and P. Bongrand. 1984. Competition between nonspecific repulsion and specific binding. *Biophys. J.* 45:1051–1064.

31. Dembo, M., D. C. Torney, K. Saxman, and D. Hammer. 1988. The reaction limited kinetics of membrane-to-surface adhesion and detachment. *Proc. R. Soc. Lond. (Biol.).* 234:55–83.

32. Smith, M. L., D. S. Long, E. R. Damiano, and K. Ley. 2003. Near-wall micro-PIV reveals a hydrodynamically relevant endothelial surface layer in venules in vivo. *Biophys. J.* 85:637–645.

33. Leyton-Mange, J., S. Yang, M. H. Hoskins, R. F. Kunz, J. D. Zahn, et al. 2006. Design of a side-view particle imaging velocimetry flow system for cell-substrate adhesion studies. *J. Biomech. Eng.* 128:271–278.

34. King, M. R., D. Bansal, M. B. Kim, and I. H. Sarelius. 2004. The effect of hematocrit and leukocyte adherence on flow direction in the microcirculation. *Ann. Biomed. Eng.* 32:803–814.

35. Faust, N., F. Varas, L. M. Kelly, S. Heck, and T. Graf. 2000. Insertion of enhanced green fluorescent protein into the lysozyme gene creates mice with green fluorescent granulocytes and macrophages. *Blood.* 96:719–726.

36. Bosse, R., and D. Vestweber. 1994. Only simultaneous blocking of the L- and P-selectin completely inhibits neutrophil migration into mouse peritoneum. *Eur. J. Immunol.* 24:3019–3024.

37. Baez, S. 1973. An open cremaster muscle preparation for the study of blood vessels by in vivo microscopy. *Microvasc. Res.* 5:384–394.

38. Ley, K., and T. F. Tedder. 1995. Leukocyte interactions with vascular endothelium. New insights into selectin-mediated attachment and rolling. *J. Immunol.* 155:525–528.

39. Kunkel, E. J., U. Jung, D. C. Bullard, K. E. Norman, B. A. Wolitzky, et al. 1996. Absence of trauma-induced leukocyte rolling in mice deficient in both P-selectin and intercellular adhesion molecule 1. *J. Exp. Med.* 183:57–65.

40. Pickard, J.E., and K. Ley. 2007. Shear field around adherent leukocytes as measured by Micro-PTV. *In* Signals, Systems and Computers, 2007. Conference Record of the Thirty-Eighth Asilomar Conference on Signals, Systems and Computers.

41. Cheezum, M. K., W. F. Walker, and W. H. Guilford. 2001. Quantitative comparison of algorithms for tracking single fluorescent particles. *Biophys. J.* 81:2378–2388.

42. Chapman, G. B., and G. R. Cokelet. 1998. Flow resistance and drag forces due to multiple adherent leukocytes in postcapillary vessels. *Biophys. J.* 74:3292–3301.

43. Pries, A. R., T. W. Secomb, and P. Gaehtgens. 1996. Biophysical aspects of blood flow in the microvasculature. *Cardiovasc. Res.* 32:654–667.

44. Vink, H., and B. R. Duling. 1996. Identification of distinct luminal domains for macromolecules, erythrocytes, and leukocytes within mammalian capillaries. *Circ. Res.* 79:581–589.

45. Reneman, R. S., B. Woldhuis, M. G oude Egbrink, D. W. Slaaf, and G. J. Tangelder. 1992. Concentration and velocity profiles of blood cells in the microcirculation. *In* Advances in Cardiovascular Engineering. Plenum Press, New York. 25–40.

46. Sugihara-Seki, M., and G. W. Schmid-Schoenbein. 2003. The fluid shear stress distribution on the membrane of leukocytes in the microcirculation. *J. Biomech. Eng.* 125:628–638.

47. Nobis, U., A. R. Pries, G. R. Cokelet, and P. Gaehtgens. 1985. Radial distribution of white cells during blood flow in small tubes. *Microvasc. Res.* 29:295–304.

48. Sugihara-Seki, M., and R. Skalak. 1997. Force acting on spheres adhered to a vessel wall. *Biorheology*. 34:249–260.

49. Acton, S. T., K. Wethmar, and K. Ley. 2002. Automatic tracking of rolling leukocytes in vivo. *Microvasc. Res.* 63:139–148.

50. Tangelder, G. J., D. W. Slaaf, H. C. Tierlinck, R. Alewijnse, and R. S. Reneman. 1982. Localization within a thin optical section of fluorescent blood platelets flowing in a microvessel. *Microvasc. Res.* 23:214–230.

51. Damiano, E. R., D. S. Long, and M. L. Smith. 2004. Estimation of viscosity profiles using velocimetry data from parallel flows of linearly viscous fluids: application to microvascular haemodynamics. *J. Fluid Mech.* 512:1–19.

52. Chapman, G. B., and G. R. Cokelet. 1997. Model studies of leukocyte-endothelium-blood interactions. II. Hemodynamic impact of leukocytes adherent to the wall of post-capillary vessels. *Biorheology*. 34:37–56.

53. Savery, M. D., and E. R. Damiano. 2008. The endothelial glycocalyx is hydrodynamically relevant in arterioles throughout the cardiac cycle. *Biophys. J.* 95:1439–1447.

54. Dong, C., J. Cao, E. J. Struble, and H. H. Lipowsky. 1999. Mechanics of leukocyte deformation and adhesion to endothelium in shear flow. *Ann. Biomed. Eng.* 27:298–312.

55. Lei, X., M. B. Lawrence, and C. Dong. 1999. Influence of cell deformation on leukocyte rolling adhesion in shear flow. *J. Biomech. Eng.* 121:636–643.

56. Gaver, III, D. P., and S. M. Kute. 1998. A theoretical model study of the influence of fluid stresses on a cell adhering to a microchannel wall. *Biophys. J.* 75:721–733.

57. Schmid-Schoenbein, G. W., D. W. Slaaf, S. I. Simon, and R. L. Engler. 1987. The interaction between leukocytes and endothelium in vivo. *Ann. N.Y. Acad. Sci.* 516:348–361.